DEVELOPMENT AND APPLICATION OF ENGINEERING TRANSITION MODEL FOR ROTORCRAFT AERODYNAMICS

J. L. Hill and S. T. Shaw
Department of Aerospace Sciences, School of Engineering, Cranfield University,
Cranfield, United Kingdom

N. Qin
Department of Mechanical Engineering, Sheffield University
Sheffield, United Kingdom

Abstract

A method for computing low Reynolds number flows containing laminar-turbulent transition is described. The model employs empirical relationships to describe the onset and extent of transition and is coupled with a two equation turbulence model. The model is applied to study laminar-turbulent transition problems related to helicopter aerodynamics. Results are presented for steady two-dimensional low Reynolds number aerofoil flows, two-dimensional dynamic stall of pitching aerofoils and the three-dimensional flow around a two bladed rotor in hovering flight.

1. Introduction

The behaviour of the boundary layer on rotating wings has been an area of great interest for rotor and propeller aerodynamicists for many years. Boundary layers have a profound effect on the performance and capabilities of the rotor, strongly influencing the drag generated and the maximum attainable lift. In the case of the helicopter rotor, boundary layer transition is of particular importance since the accurate prediction of rotor torque and hence power is essential in the design of new rotorcraft. In addition, one of the principle limitations of the maximum attainable forward flight speed and high speed manoeuvrability of helicopters is the onset of dynamic stall. Dynamic stall in which separation is initiated at the leading edge is known to be particularly sensitive to transitional flow.

Inclusion of transition within simulations based upon solution of the Reynolds averaged Navier-Stokes equations is challenging. Transition physics, mathematical tools for boundary layer stability analysis and progress made in transition prediction were reviewed by Malik [1] who identified four instability modes, Tollmien-Schlichting, Gortler, cross-flow and Mack. The relative importance of the individual instability modes in the flow around helicopter rotors is poorly understood. However, in the context of the present paper we believe that the Tollmien-Schlichting instability is predominant and focus our effort on the modelling of this mode.

Cebeci [2] highlighted the basic ingredients required to incorporate transition within Reynolds averaged Navier-Stokes simulations. These are the determination of transition onset, the length of transition and modifications to the turbulence model to accommodate the presence of the laminar and transitional flow regimes. The latter has commonly been achieved by direct manipulation of the turbulent viscosity while two alternate strategies, empiricism or stability analysis, for the prediction of transition onset and extent can be identified.

Ekaterinaris and his co-workers [3] employed empirical models for transition onset, namely, Michel's criterion [4], and solutions of the thin-layer Navier-Stokes equations to study the development of laminar separation bubbles on a NACA 0012 aerofoil. Comparisons of the computed data with pressure distributions derived from optical measurements show that inclusion of a representation of the transition physics is crucial to the improving predictive capability.

Bertagnolio *et al.* [5] evaluated Michel's model for a wide range of low Reynolds number aerofoils. Comparisons of predicted and measured transition locations were generally favourable. However, the data suggest that Michel's criterion performs poorly for aerofoils with sharp leading edges, such as the NACA 63-430. Bertagnolio relates this poor performance to the insensitivity of Michel's criterion at the leading edge suction peak. Failure of the model to predict transition at the suction peak is compounded by a relatively benign pressure gradient that further delays transition. This spurious behaviour is resolved by adjusting the model coefficients so that transition is predicted at the measured locations.

Methods based on stability analysis are generally based on the e^n method proposed independently by Smith [6] and Van Ingen [7,8]. In the e^n method the laminar boundary layer equations are solved for a given pressure distribution and the velocity distributions calculated. The stability properties of the velocity distributions are then examined through solution of the Orr-Sommerfeld equation.

Stock [9] successfully coupled an e^n method with two-dimensional solutions of the Navier-Stokes

equations. The coupling procedure is indirect involving three-stages; an evaluation of the pressure distribution by solution of the Reynolds averaged Navier-Stokes equations, an evaluation of the boundary layer properties by solution of laminar boundary layer equations and finally evaluation of the transition location using the Orr-Sommerfeld equation.

Johansen and Sorenson [10] compared transition predictions obtained using an empirical model with those obtained using a simplified e^n method. The predicted transition location obtained from the e^n method was generally further downstream than that obtained using the empirical model although both methods compare favourably with measured two-dimensional data. Based upon such comparisons the additional expense and complexity of the e^n method appear unwarranted.

The application of transition modelling to problems in helicopter aerodynamics has been limited. Ekaterinaris and his co-workers [11,12] employed empirical models for transition onset, namely, Michel's criterion [4], and solutions of the thin-layer Navier-Stokes equations to study the development and progression of dynamic stall on a on a NACA 0012 aerofoil. Subsequently Hill, Shaw and Qin [13] examined the role of transition modelling in dynamic stall computations while Geissler [14] employed a transition model in his study of leading edge flow control for low-speed dynamic stall. In these studies comparisons of the computed data of with measurements show that inclusion of a representation of the transition physics is crucial to improving predictive capability.

More recently Hill, Shaw and Qin [15] have explored the use of empirical models in the prediction of transition for isolated rotors in hovering flight. In their study it was assumed that the influence of spanwise instabilities could be neglected and a two-dimensional model was applied at each spanwise station. Comparison of the computed data with corresponding two-dimensional calculations appeared to confirm experimental observations regarding the two dimensional nature of transition for isolated hovering rotors.

In this paper we review the development and application of an empirical approach to the prediction of transitional flows of interest in helicopter aerodynamics. Empirical models have been employed to predict the location and extent of transition due to Tollmien-Schlicting instability and separation. The model provides an intermittency distribution that is used to attenuate the terms governing the production and destruction of turbulent kinetic energy and turbulent dissipation in the two-equation turbulence model employed. The model is used to compute low Reynolds number flow around the NACA 0012 and Aerospatiale A aerofoils, for attached and separated flows around pitching aerofoils and for transitional flow around an isolated helicopter main rotor in hovering flight.

2. Numerical Method

The governing equations are the Reynolds-averaged Navier-Stokes equations together with the k-ω turbulence models described by Wilcox [16] and Menter [17]. These equations can be written in the integral-conservation form,

$$\int_{\Omega} Q d\Omega + \int_{S} \vec{F} \cdot \vec{n} dS = \int_{\Omega} \vec{H} d\Omega \qquad (1)$$

in which Q is the vector of conserved variables, $\vec{F}$ is the flux function, $\vec{n}$ is the outward pointing unit vector normal to the volume surface and $\vec{H}$ is a source term arising from the turbulence model. The fluid is assumed to be a Newtonian perfect gas and Sutherland's law is employed to model the coefficients of viscosity and thermal conduction.

Spatial discretization of the governing equations is performed using a nominally third-order accurate Godunov scheme based upon the approximate Riemann solver described by Osher and Solomon [18]. The viscous fluxes are evaluated using a second-order finite volume approach in which derivatives are evaluated using Gauss's theorem.

The discretized equations are marched in time using a closely coupled implicit method in which the mean flow and the turbulent flow equations are solved simultaneously. Local time-stepping is utilized to accelerate convergence to the steady state for steady problems while a second order time accurate method based upon the pseudo-time approach is utilized for time-dependent calculations.

This method has proven to be accurate, efficient and robust for a wide class of problems, see for example [19],[20],[21] and [22].

3. Transition Model

In order to accommodate the presence of transitional flow in the current calculations a transition model is employed. The transition model consists of three key elements; prediction of transition onset, prediction of the transition length and a method for using this information to control the behaviour of the turbulence model.

3.1 Transition Onset The empirical criteria reported by Michel [4] are used in the present work to describe the location of transition due to the growth of Tollmien-Schlichting instabilities. In this model transition is

assumed to occur when the local Reynolds number based upon the momentum thickness exceeds a critical value determined by the equation,

$$\mathrm{Re}_{\theta,tr} = 2.9\,\mathrm{Re}_{x,tr}^{0.4} \qquad (2)$$

in which Re_θ and Re_x are the local Reynolds numbers based on momentum thickness and distance from the aerofoil leading edge respectively. The model requires knowledge of both the velocity at the boundary layer edge and the boundary layer momentum thickness.

Calculation of Momentum Thickness The parameters employed in Michel's empirical model are those corresponding to a laminar boundary layer. Unfortunately this data may not be readily available from the Navier-Stokes solution. The basic problems are illustrated in Figure (1), which shows calculated distributions of Reynolds number based on momentum thickness for two-boundary layers tripped at different chord-wise locations (12% and 20% chord).

As expected, Figure (1) shows a rapid growth in momentum thickness immediately following the onset of transition, reflected in a near instantaneous change in gradient of the curve. This behaviour has the effect of inhibiting the movement of the transition point aft of the initial transition location into the transitional region as the solution converges towards a steady state. In addition, there is evidence of upstream influence of the transitional and fully turbulent flow regimes, which may produce non-trivial changes in the computed boundary layer upstream of the transition location. These problems may lead to erroneous predictions of transition location when the method is used interactively for steady flow computations or when used to

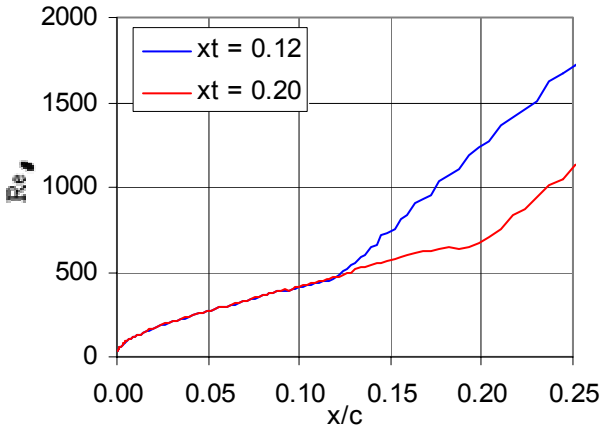

Figure (1): Computed behaviour of Reynolds number based on momentum thickness following transition to turbulent flow

model the boundary layer development on moving surfaces.

In order to overcome these problems it is necessary to model the behaviour of an *equivalent* laminar boundary layer using information from the Navier-Stokes solution. In the present work this is achieved using Thwaites method [23] in which the development of the local momentum thickness for an incompressible is related to an integration of the velocity distribution at the boundary layer edge,

$$\theta(x)^2 \approx \frac{0.45\upsilon}{u^6}\int_0^x u^5\,dx \qquad (3)$$

In order to predict transition using Michel's method we now require only the velocity distribution along the edge of the boundary layer from the CFD solution.

Determination of velocity distribution Although the complete velocity field is known at every iteration of the time marching procedure the edge of the boundary layer is generally ill-defined. This problem is evident from the irregularity of the predicted momentum thickness distributions shown in Figure (2).

For incompressible potential flows the relationship between the external pressure distribution and the velocity along the boundary layer edge can be expressed through,

$$u = U_\infty\sqrt{1 - C_p} \qquad (4)$$

If we further assume that the boundary layer is thin then from boundary layer theory we have,

$$\frac{\partial P}{\partial y} = 0 \qquad (5)$$

which in conjunction with (4) allows the velocity distribution along the boundary layer edge to be related directly to the surface pressure distribution.

Adoption of this procedure provides significant advantages over direct computation of the boundary layer edge that greatly improve the reliability and robustness of the method. In contrast to the boundary layer profiles the pressure distribution converges rapidly to the final solution. Furthermore, the surface pressure distribution, in contrast to the boundary layer velocity distribution, is relatively insensitive to the choice of grid.

Separation Model Michel's criterion applies to attached laminar boundary layers with and without pressure gradient. The model fails for flows involving laminar separation. The current method is extended to

deal with the possibility of a laminar separation region through the use of a separation model. Krumbien [24] proposes fixing transition at the computed transition location. While this procedure is generally straight forward to implement it typically predicts transition ahead of the expected location. Several empirical models for transition within separation bubbles have been reported in the literature. In the present work we employ the model described by Schmidt [25],

$$x_{tr} = \frac{2175}{u_s}\theta_s^{0.5150} \tag{6}$$

in which the location of transition is related to the momentum thickness based on distance from the separation point.

3.2 Extent of the Transition Region The extent of the transition region and the corresponding intermittency are evaluated using the empirical model presented by Walker [26]. In this model the length of the transition regime is determined from the solution of,

$$\mathrm{Re}_{l_{tr}} = 5.2\left(\mathrm{Re}_{x_{tr}}^{\frac{3}{4}}\right) \tag{7}$$

and the intermittency is determined from,

$$\chi(x) = 1 - e^{-4.65\left(\frac{x-x_{tr}}{l_{tr}}\right)} \tag{8}$$

Forward of the predicted transition location the intermittency is set to,

$$\chi(x) = 0 \quad x < x_{tr} \tag{9}$$

while aft of the transition region intermittency is given by,

$$\chi(x) = 1 \quad x > x_{turn} \tag{10}$$

3.3 Modifications to the Turbulence Model Wilcox [27] has shown that low Reynolds number formulations of the k-ω turbulence model are capable of predicting transition like phenomena in the absence of an explicit transition model, see for example Figure (2) which shows computed contours of the turbulent Reynolds number Re_T obtained using the low Reynolds number without transition model. This capability is achieved through attenuation of the production of turbulent kinetic energy and specific dissipation by the low Reynolds number model terms. The predicted location of transition is generally far aft of the measured location. Manipulation of the freestream boundary conditions can improve predicted transition location dramatically but this is at the expense of incorrect boundary layer development at the lifting surface.

In order to accommodate the presence of the laminar and transitional regions in the current computations we adopt a similar, if less rigorous, approach in which the production terms appearing on the right-hand side of Equation (1) are attenuated by the calculated intermittency. Thus the production terms are calculated from,

$$\begin{aligned} P_k &= \chi P_k' \\ P_\omega &= \chi P_\omega' \end{aligned} \tag{11}$$

where the use of $'$ indicates the unmodified term and the intermittency is provided by Equations (8)-(10).

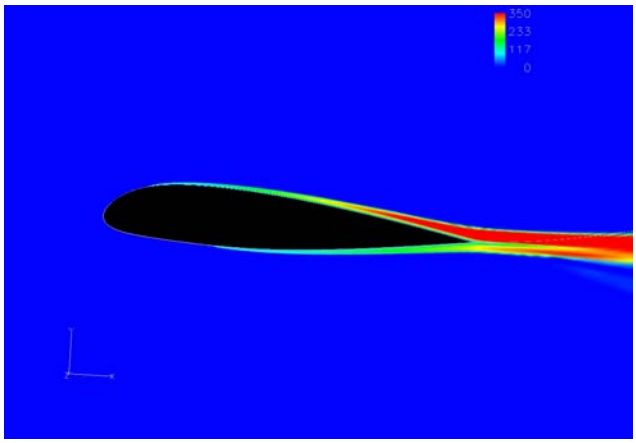

Figure (2): Contours of turbulent Reynolds number obtained using Wilcox Low Reynolds Number turbulence model

4. Steady Results

Results are first presented for steady two-dimensional flows over the NACA 0012 and Aerospatiale A- aerofoils at low Reynolds numbers. These computations provide an opportunity to assess the performance of the model for flows involving transition due to the growth of Tollmien-Schlichting instabilities and laminar separation.

The calculations were performed on structured grids which were adapted to the computation of boundary layer flows. Numerical experiments demonstrate that the present computations are grid converged.

4.1 NACA 0012 Aerofoil (High-Reynolds Number) Calculations were initially performed for a NACA 0012 aerofoil at a Reynolds number of Re_c = 2,900,000 and

a freestream Mach number of M = 0.15, this corresponds to the experiment of Gregory [28]. The transition model was used in an interactive fashion, i.e. the transition location was updated every iteration of the time marching procedure. Computed and measured transition locations are compared in Figure (3).

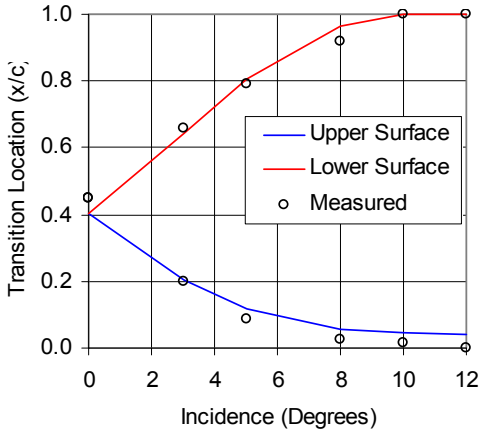

(a) Standard k-ω Model

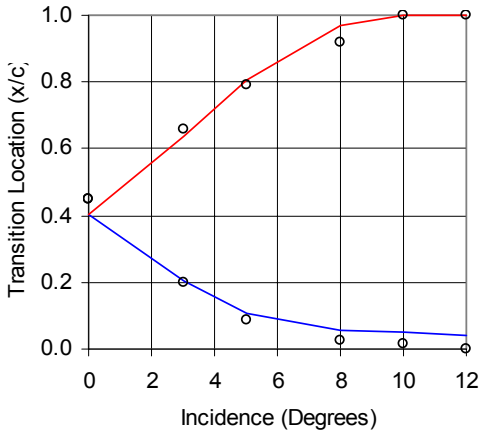

(b) k-ω SST Model

Figure (3) Comparison of computed and measured transition locations for NACA 0012 aerofoil M = 0.15 and Re_c = 2,900,000

For the incidence range considered transition on both the upper and lower surfaces is initiated by Michel's criterion (TS mode). Agreement between the computed and measured data is considered good at lower incidence. At higher incidence the computed transition location is generally aft of that measured in the experiment but the predictions remain acceptable. No significant differences are observed between the computations employing the standard k-ω model and Menter's k-ω SST turbulence model.

4.2 NACA 0012 Aerofoil (Low-Reynolds Number)

More recently detailed measurements of the low Reynolds flow over a NACA 0012 aerofoil have been performed by Favier and his co-workers at LABM; see for example references [29] and [30]. Detailed boundary layer measurements were taken for both steady and unsteady (oscillating in pitch) flows which included records of the onset and completion of transition.

Here we consider the steady flow at a Reynolds number of Re_c = 100,000 and a Mach number of M = 0.15 over the incidence range studied experimentally. Figure (4) compares the computed location of transition onset and completion with the measured data.

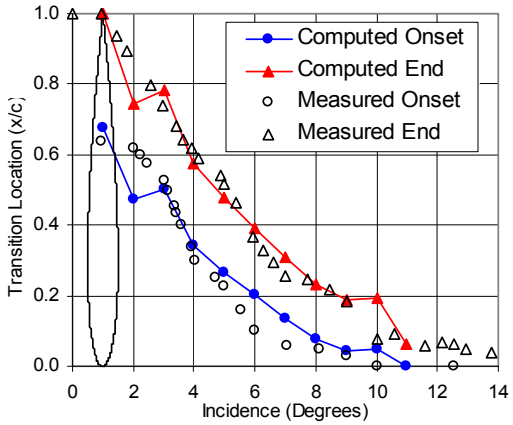

(a) Standard k-ω Model

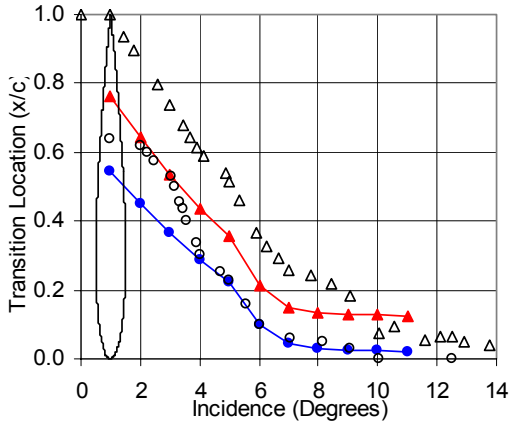

(b) k-ω SST Model

Figure (4) Comparison of computed and measured upper surface transition locations for NACA 0012 aerofoil M = 0.15 and Re_c = 100,000

Comparison of the computed and measured data is considered fair. In general the standard k-ω model appears to perform better at predicting transition onset at lower incidences while there is significant

improvement for the separated flows at higher incidence using the k-ω SST model. The predicted transition length appears shorter in the SST model predictions compared to the standard model predictions. The computations indicate the presence of laminar separation and turbulent re-attachment over much of the incidence range. At low incidences the separation is towards the mid-chord but moves forward as incidence is increased. For a narrow range of incidences (4° to 8°) the flow remains fully attached and transition is initiated through the Tollmien-Schlichting instability mode. Beyond 8° of incidence, separation (and consequently transition) occurs close to the leading edge.

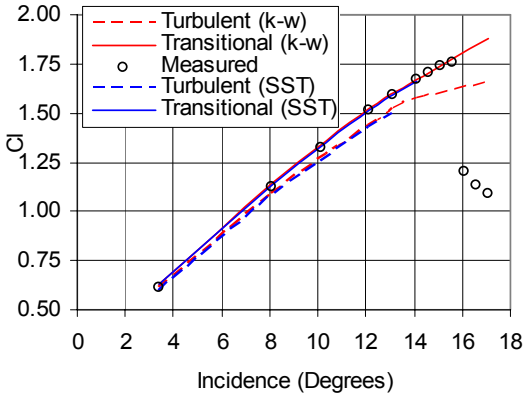

(a) Variation of lift coefficient with incidence

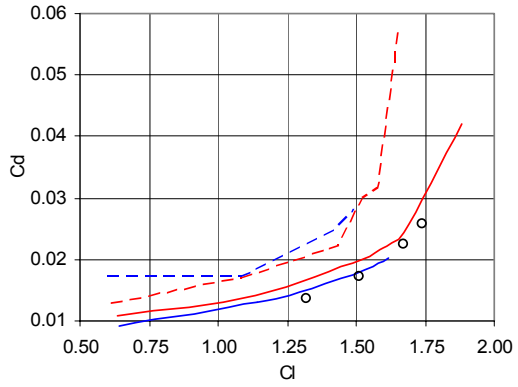

(b) Lift – Drag Polar

Figure (5) Comparison of fully turbulent and transition free computations Aerospatiale A-aerofoil M = 0.15 and Re_c = 3,130,000

Results from fully turbulent calculations at this Reynolds number and Mach number indicate that the flow remains fully attached below 8° of incidence. Above this angle separation occurs, but in contrast to the free transition simulations separation is initiated at the aerofoil trailing edge and moves forwards as incidence is increased further. This contrast in physical behaviour between results obtained from the fully turbulent and free-transition simulations illustrates the importance of modelling transition physics at lower Reynolds numbers.

4.3 A-Aerofoil The final steady two-dimensional test case relates to the flow around the Aerospatiale A Aerofoil. This aerofoil has been the focus of an extensive European CFD validation effort [31]. Measurements include surface pressure coefficients, skin friction distributions and detailed boundary layer measurements.

Computations were performed for two Reynolds numbers, Re_c = 3,130,000 (F1) and Re_c = 2,000,000 (F2) and a Mach number of 0.15 on the common fine grid provided in [31]. This grid contains 513 points around the aerofoil and 129 in the direction normal to the surface.

The variations of lift with incidence from fully turbulent calculations and free transition calculations are compared with experimental measurements at a Reynolds number of 3,130,00 in Figure (5). Also shown are the corresponding lift-drag polars. Use of the transition model improves agreement between the experimental and calculated lift coefficient significantly with excellent agreement observed between the computed and measured data over much of the incidence range. Use of the model also improves agreement between the computed and measured drag coefficients although the comparison remains poor when using the standard k-ω turbulence model. Further significant improvements are obtained using Menter's k-ω SST model.

Figure (6) is typical of the improvements between calculated and measured pressure and skin friction distributions that can be achieved using the present approach to transition together with the standard k-ω model. Improvements in computed pressure coefficient are generally confined to the leading edge region where significant improvements in the prediction of the leading edge suction are evident. This observation is the principal reason for improvements in computed lift coefficient. Comparisons of computed and measured skin friction distribution suggest that the transition location is well predicted (transition location was not measured in the experiment). The resulting reduction in skin friction in the leading edge region provide an explanation for the reduction in drag coefficient observed between fully turbulent and transition free calculations.

Finally computed boundary layer profiles obtained using the standard k-ω model are compared with data from the F2 experimental data set at incidences of 7.2° and 13.3° in Figure (7) and (8) respectively. The agreement is considered good with significant

improvements obtained as a result of the transition modelling.

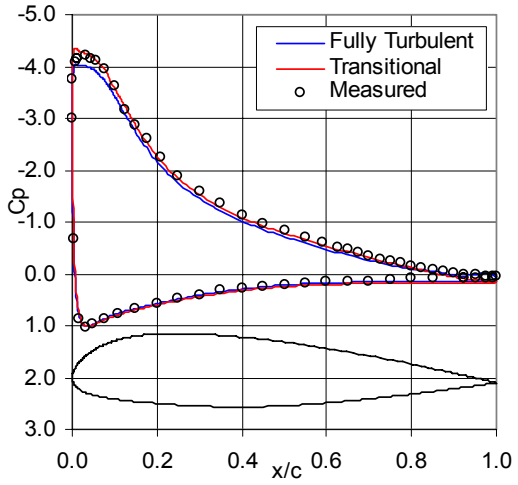

(a) Pressure distribution

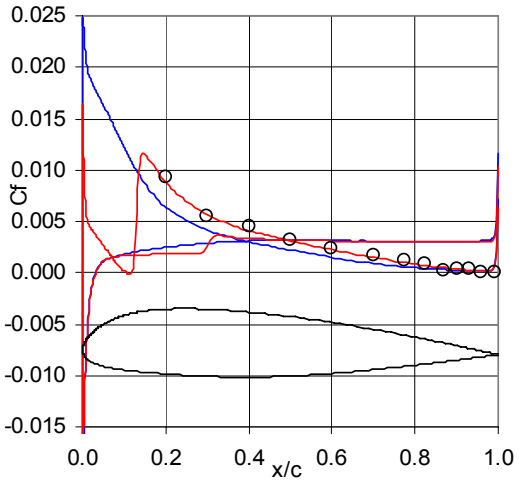

(b) Skin friction distribution

Figure (6) Comparison of fully turbulent and transition free computations Aerospatiale A-aerofoil M = 0.15 and Re_c = 3,130,000

5. Unsteady Results

Dynamic stall phenomena are important in many fields of aerospace science including turbo-machinery, wind turbines and manoeuvring fixed wing aircraft. In rotorcraft engineering a detailed understanding of the unsteady air-loads acting on the moving blades is essential for the prediction of rotor performance, rotor dynamics (including blade aero-elastics) and noise generation in forward flight.

Much of our understanding of dynamic stall has come through careful experimentation on single element aerofoil configurations using pitching oscillations to generate the required unsteadiness. Reviews of progress in the experimental understanding of dynamic stall phenomena have been presented by Carr [32] and Carr and Chandrasekhara [33], The phenomenology of dynamic stall is illustrated using results from the present computations in Figure (9).

The complex nature of the phenomena has led to a range of predictive models ranging in fidelity from simple empirical models to large eddy simulations. Semi-empirical models, such as those used by Westland Helicopters [34] provide robust practical tools that can be used within the design environment. More recently rapid progress has been made in the application of numerical simulation tools to the problem of dynamic stall, see for example the reviews by Ekaterinaris [11] and [12].

The occurrence and progression of dynamic stall is sensitive to a number of parameters such as pitch rate, geometry, Mach number, amplitude and Reynolds number. Numerical methods based upon the solution of the Navier-Stokes equations generally reproduce the qualitative behaviour of the flow with respect to such parameters. For dynamic stall initiated as a result of trailing edge acceptable quantitative agreement can generally be obtained with the experimental data for all but the most severe separations using modern one- and two-equation turbulence models.

Quantitative agreement for stall initiated at the leading edge is less favourable. There is good experimental and numerical evidence, see for example the discussions of References [11] and [12] that in this case the flow is sensitive to the state of the boundary layer (laminar, transitional or fully turbulent) immediately ahead of the separation point. In order to demonstrate this we consider the transitional flow around two pitching aerofoils. In the first case the flow is attached during the pitching oscillation while in the second case dynamic stall occurs.

5.1 Attached Flow Initial calculations were performed to assess the ability of the numerical method to predict steady attached flows. Computations were performed for a NACA 0015 aerofoil performing pitching oscillations about the quarter-chord location at a Mach number of M = 0.30 and a Reynolds number Re_c = 2,000,000. The instantaneous incidence is determined from,

$$\alpha(\tau) = 4.0 + 4.2\sin(0.1\tau)$$

where τ is a non-dimensional measure of time. This motion corresponds to the experiment of Pizzali [35].

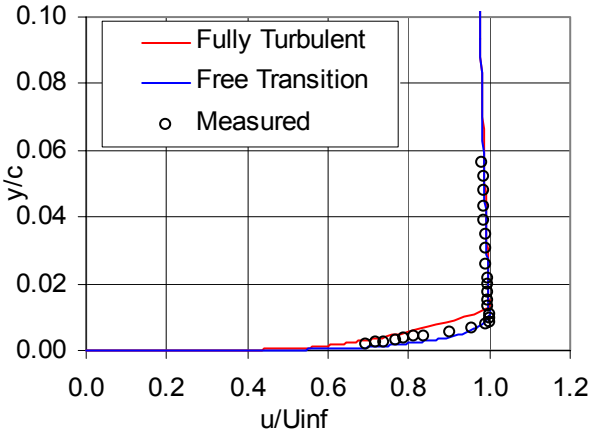

(a) x/c = 0.4

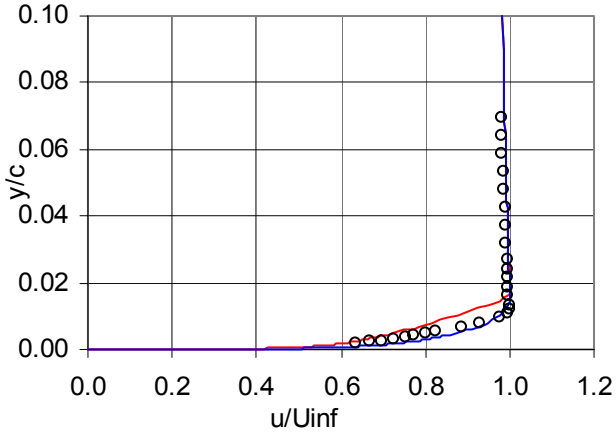

(b) x/c = 0.5

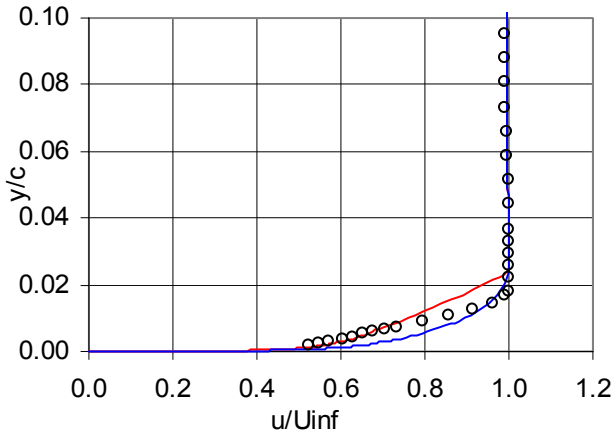

(c) x/c = 0.7

Figure (7) Comparison of fully turbulent and transition free computations Aerospatiale A-aerofoil M = 0.15, α = 7.2°and Re_c = 2,000,000

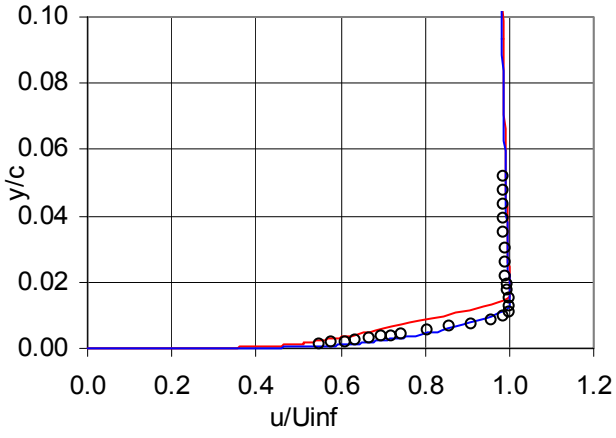

(a) x/c = 0.4

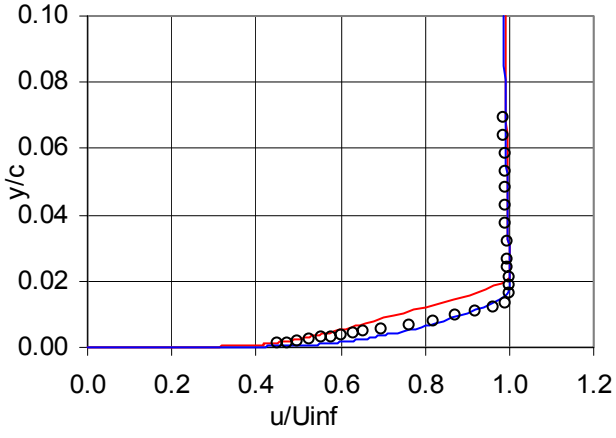

(b) x/c = 0.5

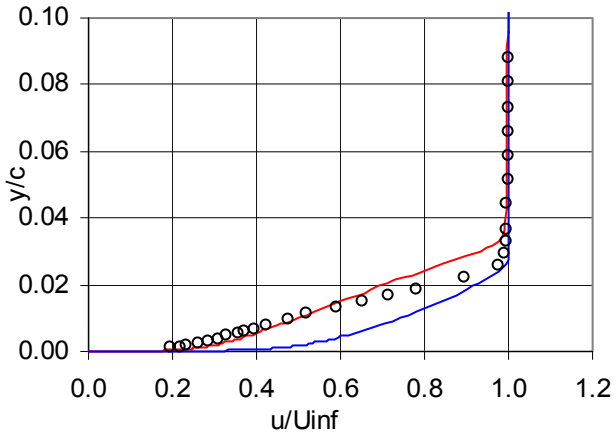

(c) x/c = 0.7

Figure (8) Comparison of fully turbulent and transition free computations Aerospatiale A-aerofoil M = 0.15, α = 13.3° and Re_c = 2,000,000

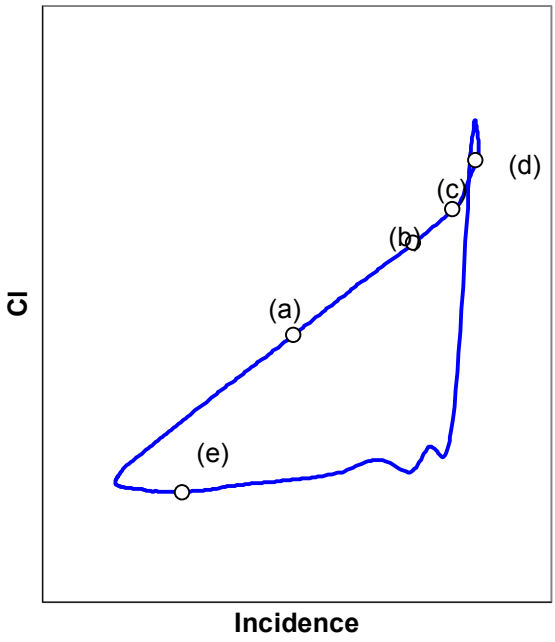

(i) Normal Force Hysterisis

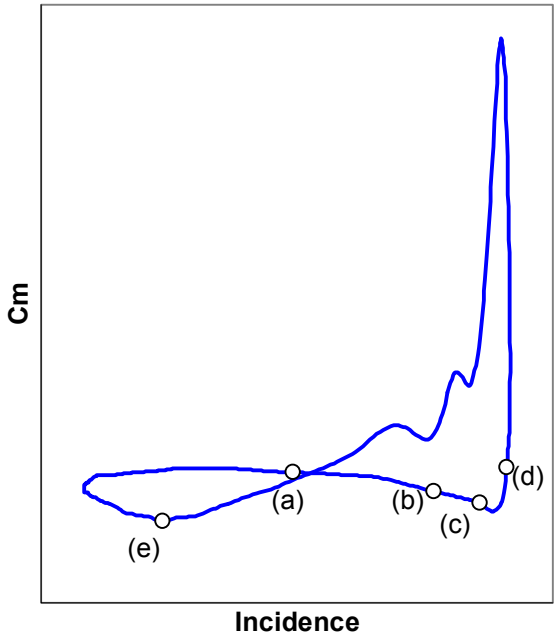

(ii) Pitching Moment Hysterisis

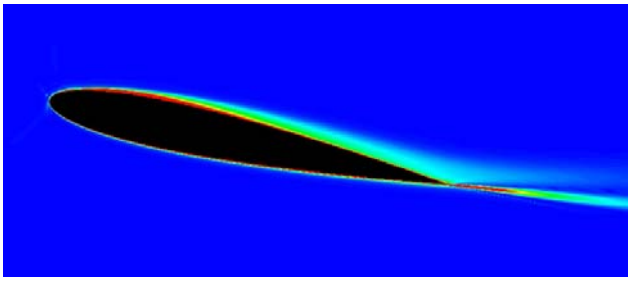

(a) Attached Flow

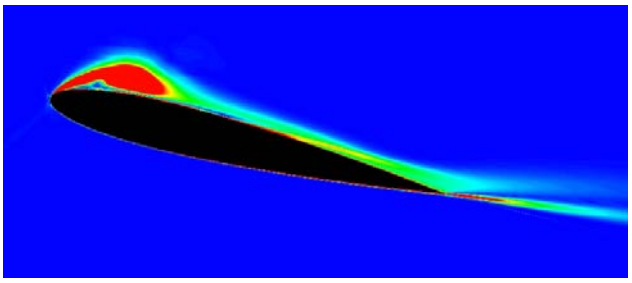

(b) Formation of Leading Edge Vortex

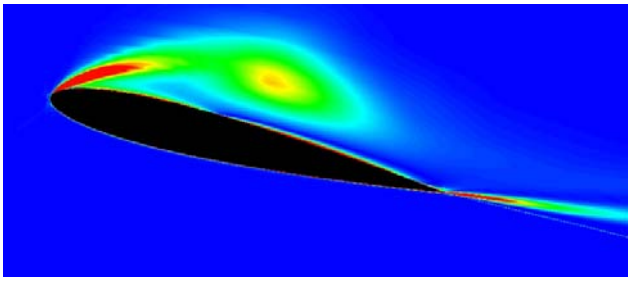

(c) Movement of Leading Edge Vortex

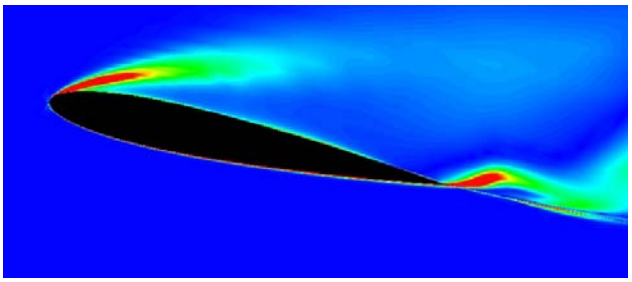

(d) Full Stall

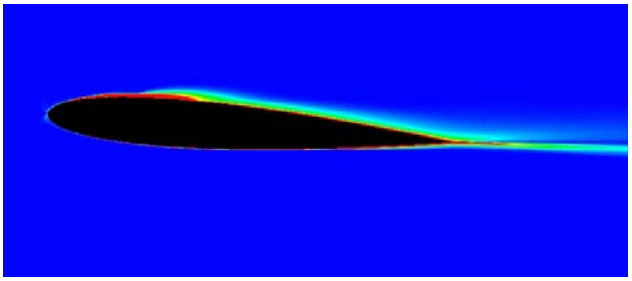

(e) Re-attachment during Down Stroke

Figure (9): Dynamic Stall Events

The computed flow is attached over the full cycle. Computed hysterisis loops for lift, drag and pitching moment coefficients obtained assuming fully turbulent flow are compared with the measurements of Pizzali in Figure (10). The computed data were obtained by integration of the instantaneous pressure distributions at each time step. Differences between the standard and SST variants of the k-ω show no significant differences for the computed lift and drag hysterisis. More significant differences are observed for the pitching moment during the down stroke. The agreement between the current calculations and the experimental data is generally favourable.

In order to investigate the sensitivity of the computed flow to transition the attached flow calculation was repeated with transition fixed and with transition fixed at two locations on the aerofoil chord. Calculations performed with transition fixed at 2.5% and 5.0% of the aerofoil chord and using the transition model and the standard k-ω model are shown in Figure (11). The inclusion of transition in the computations has a small influence on the predicted lift and drag hysterisis. The differences are small during the upstroke and more significant during the downstroke. The corresponding improvements in pitching moment, Figure (11b), are much larger. Using the transition model leads to non-trivial improvements during the upstroke. There is also a general improvement during the down stroke compared to the results obtained assuming fully turbulent flow. It is believed that these differences occurs as a result of changes in the flow behaviour on the lower surface of the aerofoil, this leads to much better predictions of the shape of the instantaneous pressure distribution with obvious implications for the integrated forces and pitching moment.

The predicted transition locations are presented in Figure (11c). There is significant hysterisis on both the upper and lower surfaces. Transition on the aerofoil upper surface ranges from around 12% of chord at the beginning of the up stroke to 40% of chord at the beginning of the down stroke. Comparing the upper surface transition location during the up stroke and down stroke it is observed that at constant instantaneous incidence transition occurs earlier during the up stroke than during the down stroke. This is attributed to the action of the aerofoil acceleration and induced effects of the shed wake on the local pressure gradients.

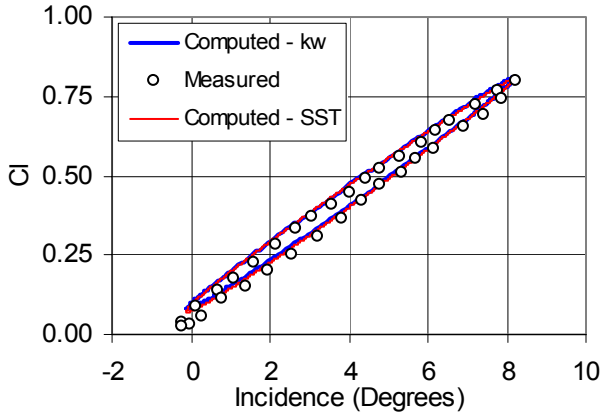

(a) Lift Coefficient

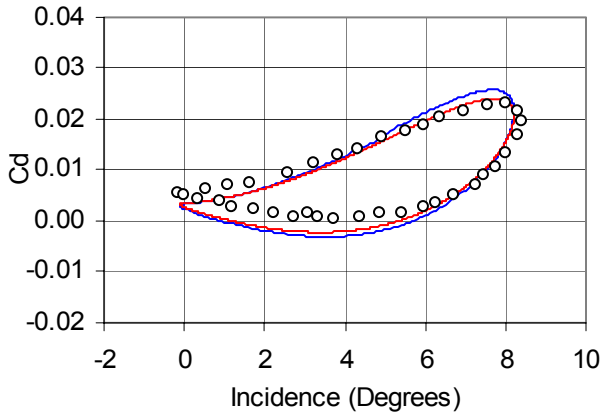

(b) Drag Coefficient

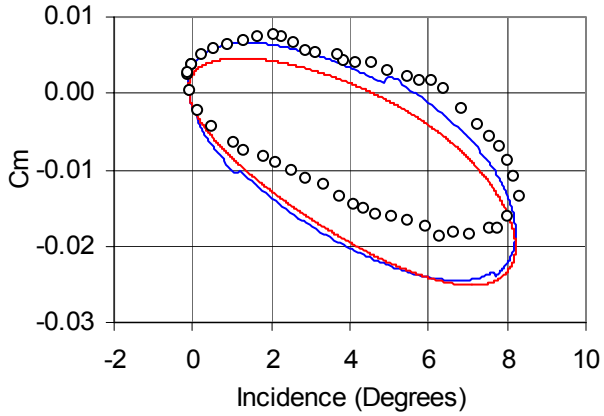

(c) Pitching Moment Coefficient

Figure (10) Comparison of computed and measured forces and moments for pitching aerofoil (fully attached turbulent flow)

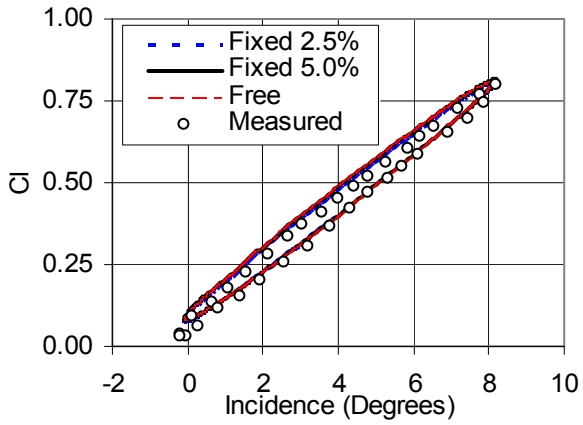

(a) Lift Coefficient

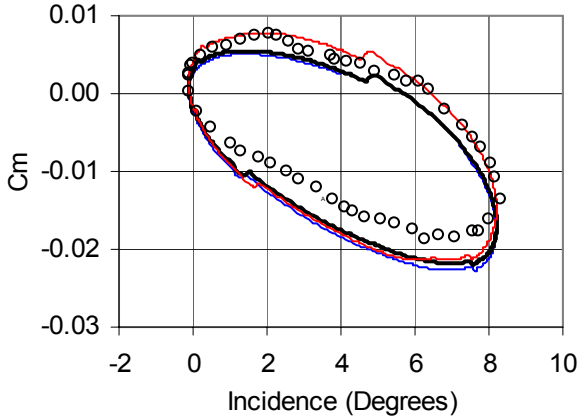

(b) Pitching Moment Coefficient

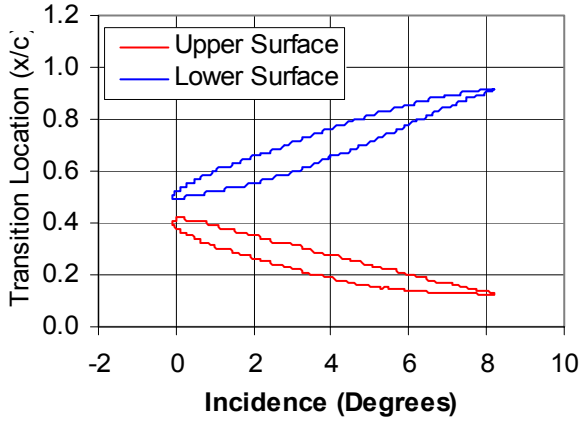

(c) Transition Location

Figure (11) Comparison of computed and measured forces and moments for pitching aerofoil (fully attached transitional flow)

5.2 Separated Flow The effect of laminar/turbulent transition on dynamic stall predictions was investigated for a NACA 0012 aerofoil performing pitching oscillations about the quarter-chord location at a Mach number of M = 0.30 and a Reynolds number Re_c = 4,000,000. The instantaneous incidence was determined from,

$$\alpha(\tau) = 9.0 + 5.0\sin(0.1\tau)$$

This motion corresponds to the experiment of McCroskey [36]. Initial computations were performed with transition fixed at the leading edge (fully turbulent) and at 5% and 10% of the aerofoil chord. The computed forces and moments are compared with the experimental measurements in Figure (12).

Figures (12) and (13) show that fully turbulent computations using the standard k-ω and k-ω SST turbulence models are unable to reproduce all of the hysterisis effects observed in the experimentally measured forces and moments. This deficiency is particularly evident in the computed lift coefficient. This behaviour is attributed to the failure of the computation to resolve the flow break down at the leading edge correctly.

For computations performed with fixed transition close to the leading edge the complexity of the experimental hysterisis is observed in the computed data although quantitative agreement remains poor. This is clearly evident in the computed lift coefficient data which indicate that movement of the transition location further aft results in increasingly heavy stall. Use of Menter's variant of the k-ω model produces a deeper stall than is observed with the standard model. This behaviour is related to the improved sensitivity of the SST model to adverse pressure gradients. Comparing the results of the fully turbulent and fixed transition computations it is evident that state of the boundary layer close to the leading edge plays an important role in the subsequent stall development. Examination of the computed pressure distributions supports this view. In the case of the fully turbulent calculation the leading edge pressure peak is maintained during the whole motion cycle, while in the fixed transition calculations the leading edge pressure collapses during the down stroke indicating laminar separation. The extent and severity of this separation is determined by the transition location.

Subsequent computations were performed for this case using elements of the transition model described earlier. Results obtained using Michel's transition criteria and Walker's description of intermittency are presented in Figure (15). The corresponding transition locations are shown in Figure (14).

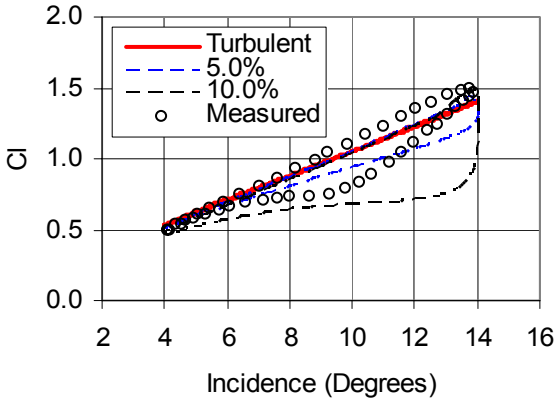

(a) Lift Coefficient

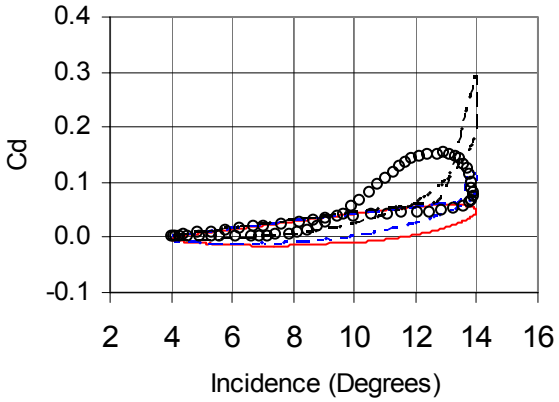

(b) Drag Coefficient

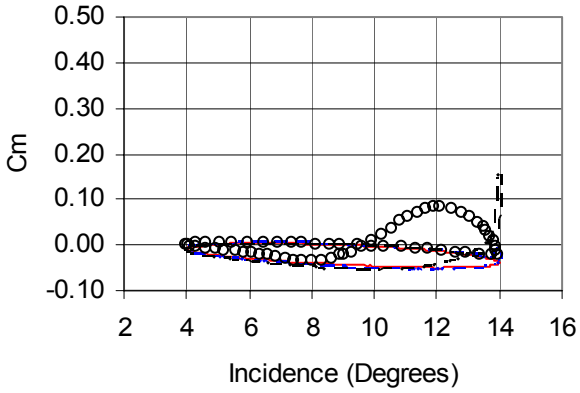

(c) Pitching Moment Coefficient

Figure (12) Influence of fixed transition on computed forces and moments for pitching aerofoil (k-ω Model)

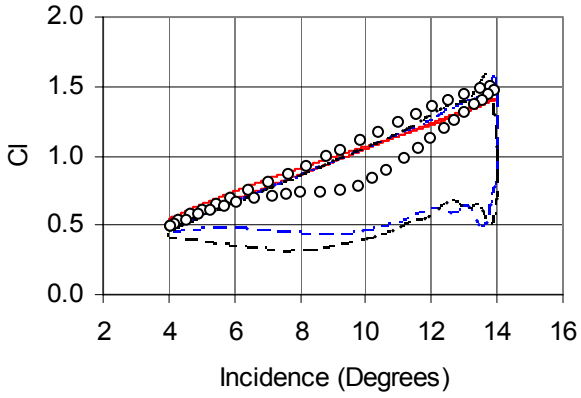

(a) Lift Coefficient

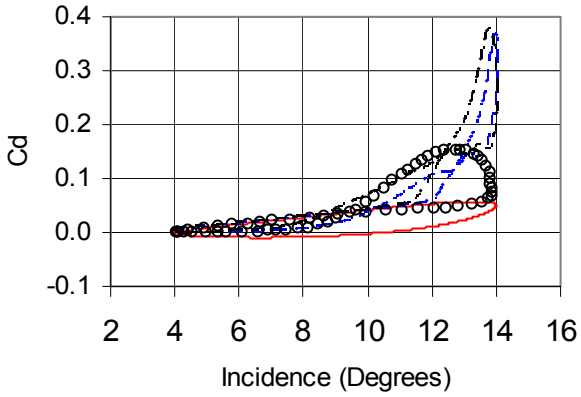

(b) Drag Coefficient

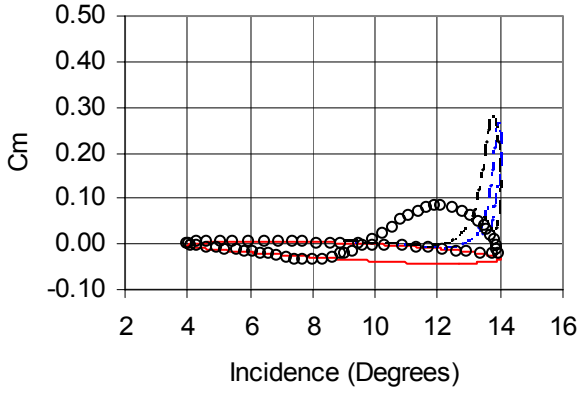

(c) Pitching Moment Coefficient

Figure (13) Influence of fixed transition on computed forces and moments for pitching aerofoil (k-ω SST Model)

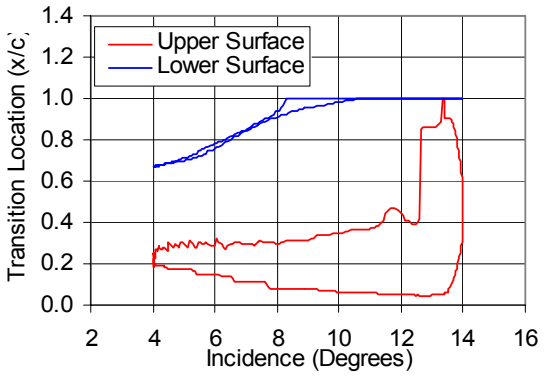

(a) k-ω Model

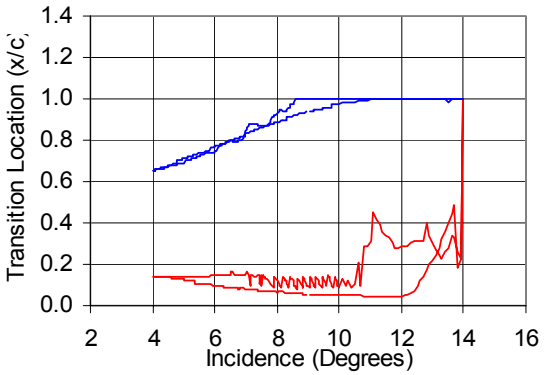

(b) k-ω SST Model

Figure (14) Predicted transition location for pitching aerofoil

The predicted upper surface transition location remains close to the leading edge during the up stroke. Following the formation and separation of the dynamic stall vortex the transition location moves towards the trailing edge. Indeed early in the down stroke the upper surface transition location moves to the aerofoil trailing edge. The importance of the aerofoil pressure distribution in determining the boundary layer profiles employed in the Michel criteria, Equation (4), is responsible for this erroneous behaviour which arise as a consequence of the collapse of the leading edge pressure following stall, see for example Figure (16).

Use of the full model appears to lead to predictions that exhibit similar behaviour to the fully turbulent calculations, see for example Figure (17) which shows the comparisons of the computed lift force with the measured experimental data. The use of the separation model appears to inhibit the development of the separated flow. In an effort to understand this behaviour further calculations were repeated with the transition location following separation fixed at 5% and 10% behind the computed separation location. Results for these

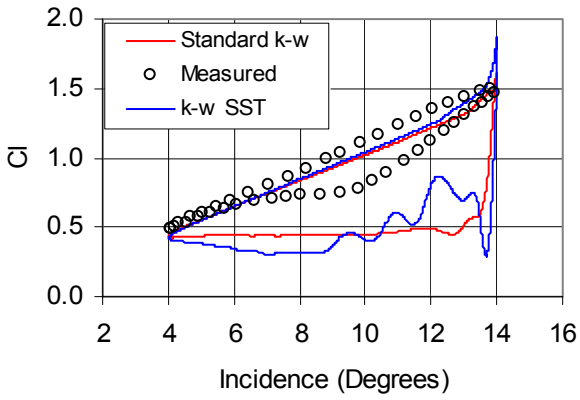

(a) Lift Coefficient

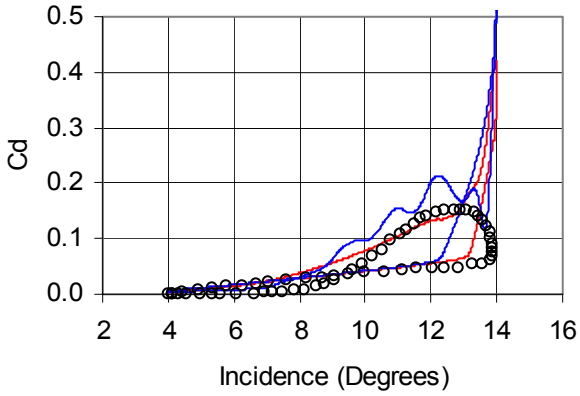

(b) Drag Coefficient

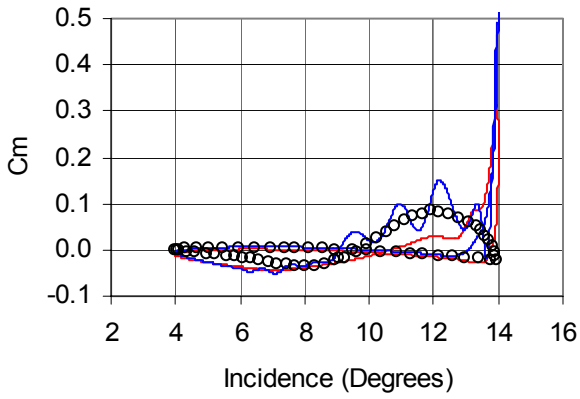

(c) Pitching Moment Coefficient

Figure (15) Influence of free transition on computed forces and moments for pitching aerofoil

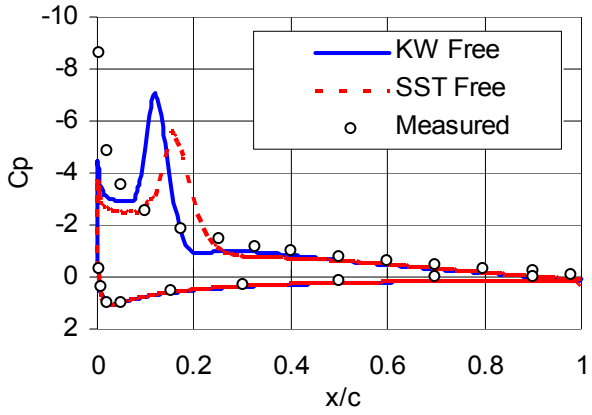

(a) $\alpha(\tau) = 13.0^{o}$ **(up stroke)**

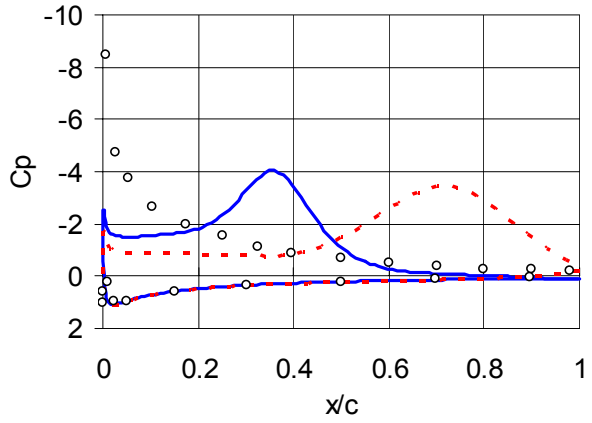

(b) $\alpha(\tau) = 14.0^{o}$

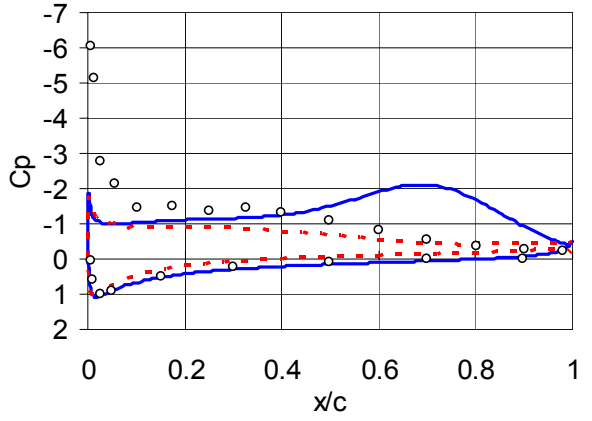

(c) $\alpha(\tau) = 13.0^{o}$ **(down stroke)**

Figure (16) Comparison of computed and measured pressure distributions for pitching aerofoil (separated flow)

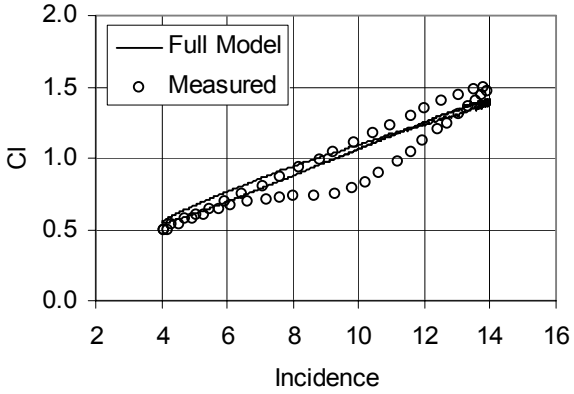

(a) k-ω Model

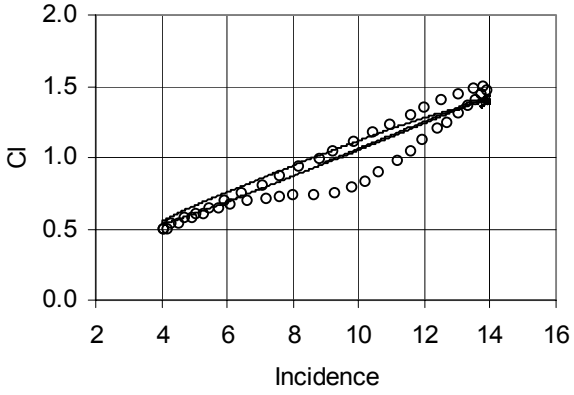

(b) k-ω SST Model

Figure (17) Influence of full transition model on computed lift force for pitching aerofoil

calculations are shown in Figure (18) for the standard k-ω model and Figure (19) for the k-ω SST model.

With transition fixed 5% and 10% of chord behind the computed separation point the k-ω SST turbulence model provides results that exhibit deep dynamic stall. The stall predicted by the standard k-ω is much milder, Figure (18) with good qualitative agreement found between the computed and measured lift forces with transition fixed 10% behind the separation point. As the distance between the transition location and separation is reduced the depth of the stall reduces in the standard model computations. Improvements in the k-ω SST model predictions can be obtained by reducing the distance between the separation point and transition location.

The sensitivity of the model to the separation length is believed to be numerical in nature. By fixing transition close to the separation location, as in the Schmitt model, the subsequent turbulent flow leads to re-attachment of the boundary layer for a time reducing significantly the development of the

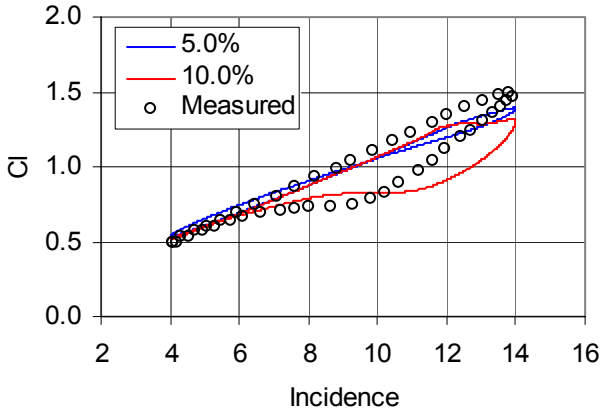

(a) Lift Coefficient

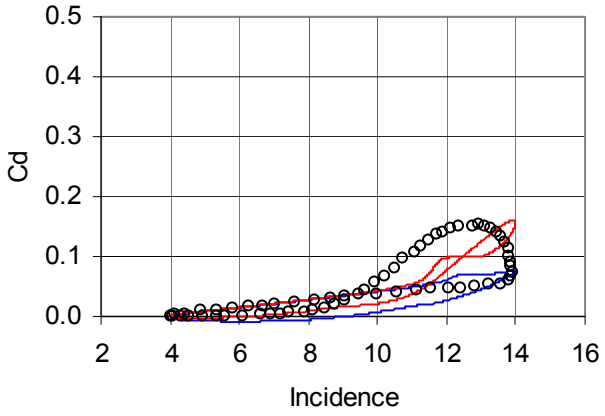

(b) Drag Coefficient

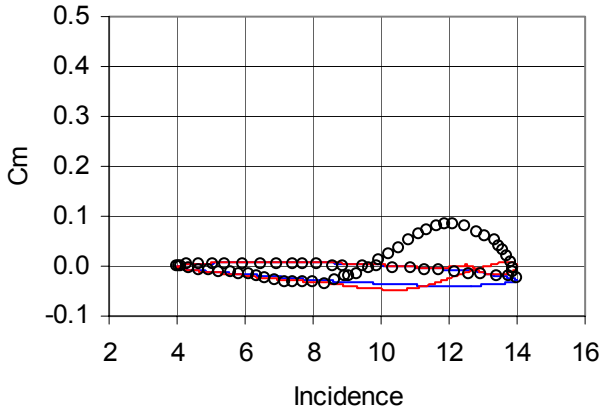

(c) Pitching Moment Coefficient

Figure (18) Influence of separation length on computed forces and moments for pitching aerofoil (k-ω model)

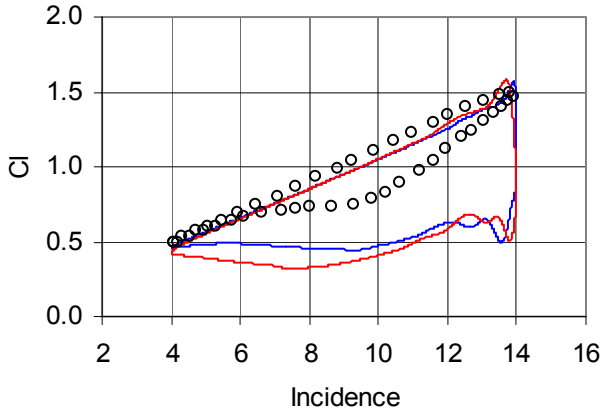

(a) Lift Coefficient

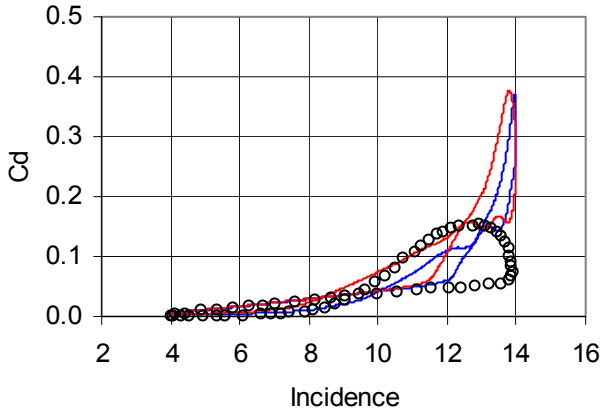

(c) Drag Coefficient

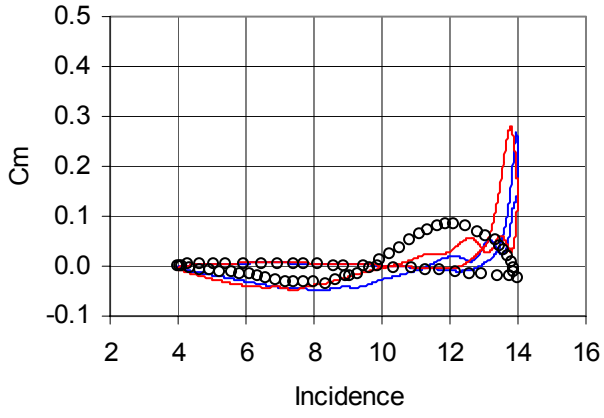

(c) Pitching Moment Coefficient

Figure (19) Influence of separation length on computed forces and moments for pitching aerofoil (k-ω SST model)

dynamic stall. Indeed with the Schmitt model the stall is almost eliminated. This behaviour is clearly non-physical and is related to the quasi-steady nature of the current model. Further work is required to resolve this issue.

6. Isolated Rotor in Hover

The final case considered is that of an isolated helicopter rotor in hovering flight. In order to demonstrate the ability of the numerical method to resolve the flow around a helicopter rotor in hovering flight, calculations were performed for an isolated two bladed rotor. The geometry consists of an untwisted rectangular blade of aspect ratio 6 with NACA 0012 cross section. The calculations were performed on structured-unstructured hybrid grids containing approximately four million cells. Although the problem is periodic both blades were modelled in the simulations. The generated grids were adapted to the expected location of the tip vortices and wake sheet, see Shaw and Hill [37] for further details. Calculations were performed at a tip Mach number of M_{tip}=0.439 and at 8° collective. This corresponds to the experiment performed by Caradonna [38].

Figure (20) presents a cross section through the grid and solution 90° behind the blade. The basic structure of the wake can be clearly identified from the vorticity contours. Several general features of the classical hovering rotor wake are evident in the computed flow. In addition to the tip vortices, which indicate that at least 450° of wake age is resolved in the simulation. Figure (20) also shows clear evidence of the wake sheet. Beyond 450° wake age the grid is no longer adapted to the flow leading to a rapid dissipation of the wake structure. Comparisons of the blade surface pressure distribution are generally good as evinced by Figure (21) which compares the spanwise loading distribution obtained from integration of the computed surface pressure coefficients with the corresponding experimental measurements.

The transition model was applied in a non-interactive fashion to the computed blade surface pressure distributions at several spanwise locations to obtain the upper and lower surface transition locations shown in Figure (22). For this rotor transition on the upper surface is predicted to occur well aft of the aerofoil leading edge suggesting that it may not be possible to justify the common assumption of fully turbulent flow used by the CFD community in Navier-Stokes simulations of helicopter rotors. As expected the upper surface transition point moves forward towards the blade leading edge as the tip is approached. This behaviour is a result of the increased local lift coefficient experienced by outboard blade sections due to increased dynamic head. There is evidence of a strong three dimensional influence close to

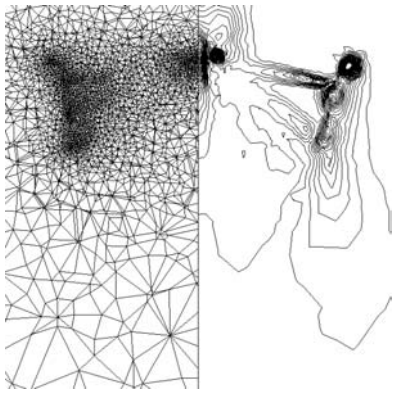

Figure (20): Cross section through computed solution and grid (ψ = 90°)

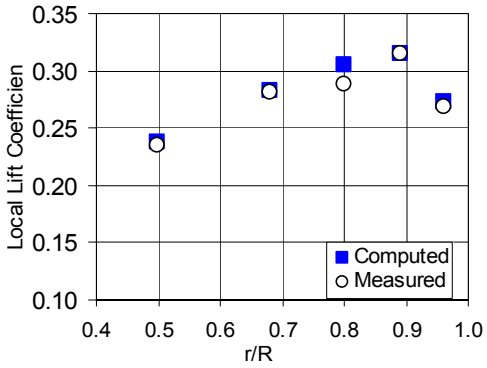

Figure (21): Comparison of computed and measured spanwise lift distributions for the Caradonna and Tung hovering rotor

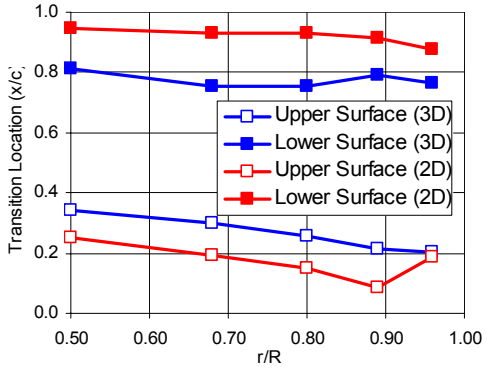

Figure (22): Computed transition locations for the Caradonna and Tung hovering rotor

the blade tip associated with reductions in tip loading (tip relief) associated with the presence of the tip vortices.

The variation of lower surface transition location is less significant than that observed on the upper

surface. Lower surface transition occurs towards the blade trailing edge between 70% and 80% chord.

Also shown in Figure (22) are the results of two-dimensional calculations performed at Mach numbers, Reynolds numbers and incidence corresponding to the local conditions experienced at 50%, 68%, 80%, 89% and 96% span. These results provide a means of assessing the influence of the rotational flow on the predicted transition location. On the upper surface the three-dimensional hover calculations consistently predict transition aft of that predicted in the two-dimensional calculations while on the lower surface the contrary situation is observed.

The results suggest that there is a significant effect of the rotating flow on the transition development which potentially has consequences for the use of two-dimensional aerofoil performance data in rotor comprehensive codes.

7. Conclusions

A method for computing low Reynolds number flows containing laminar-turbulent transition has been described. The model employs empirical relationships to describe the onset and extent of transition and is coupled with a two equation turbulence model.

Results were presented for two aerofoil configurations that demonstrate the ability of the model to compute steady attached transitional flows and flows involving leading edge separation. Comparisons of the model predictions with experimental data were generally good. The computed upper and lower surface transition locations were acceptable while computed surface pressure, skin friction and boundary layer profiles all showed significant improvement compared to fully turbulent calculations. For a fully attached unsteady flow the computed data showed only slight improvements over that obtained from fully turbulent calculations. Comparison of the computed forces and moments with experimental data was generally favourable.

For the cases considered in the present paper, the use of the transition model for unsteady separating flows provides qualitative representations of the complex force and moment hysterisis observed experimentally that could not be obtained with the assumption of fully turbulent flow. Quantitative agreement is generally poor during the down stroke with a much deeper stall predicted than was observed in the experiment.

The predicted force and moment hysterisis was shown to be sensitive to both fixed transition location and transition length. The depth of the computed stall increases as the fixed transition point moves aft or as the transitional flow region is lengthened. The movement of the upper surface transition location appears to be erroneous during the down stroke based upon quasi-steady considerations, This behaviour is attributed to deficiencies in the model relating the local velocity distribution to the computed pressure coefficients. Further work is required to improve this aspect of the model

Finally the model was applied in a non-iterative fashion to the computation of transition location on an isolated two-bladed rotor in hovering flight. The method was shown to predict transition behaviour similar to that expected from physical reasoning. Comparisons with corresponding two-dimensional predictions suggest that the influence of rotating flow is important when assessing transition location. For the three-dimensional calculations transition was generally predicted earlier on the lower surface and later on the lower surface than in the corresponding two-dimensional calculations.

Acknowledgements

The work described in this paper was supported by Westland Helicopters Ltd and the Engineering and Physical Science Research Council (EPSRC) within the HMB-UK consortium. Alan Brocklehurst (Westland Helciopters) was the technical monitor. The authors would like to acknowledge Professor Ian Poll for useful discussions and Professor D. Favier for granting permission for the use of the data generated at LABM, France.

References

1. Malik, M.R., ‘Boundary-layer transition prediction toolkit’, AIAA-1997-1904.
2. Cebeci, T., ‘Essential ingredients of a method for low Reynolds number airfoils’,AIAA J.,Vol.27 (2).
3. Ekaterinaris, J.A., Chandrasekhara, M.S. and Platzer, M.F., ‘Anaysis of low Reynolds number airfoil flows’, J. Aircraft, Vol. 32 (3), pp. 625-630.
4. Michel, R., ‘Etude de la transition sur les profile d’ aile; Edtablishment d’un critere de determination de point de transition et calcul de la trainee de profile incompressible’, ONERA Report 1/1578A, 1951.
5. Bertagnolio, F., Sorensen, N.N., Johansen, J. and Fuglsang, P., ‘Conclusions from the comparisons of numerous 2d airfoil computations with experiments’, AIAA 02-0034.
6. Smith, A.M.O., ‘Transition, pressure gradient and stability theory’, Proc. of the IX International Congress of Applied Mechanics, Vol. 4, 1956. Van Ingen, J.L., ‘A suggested semi-empirical

method for the calculation of the boundary layer region', University of Delft, Report VTH71, 1956.
7. Van Ingen, J.L., 'A suggested semi-empirical method for the calculation of the boundary layer region', University of Delft, Report VTH74, 1956.
8. Stock, H.W., 'Airfoil validation using coupled Navier-Stokes and e^n transition prediction methods', J. Aircraft, Vol. 39 (1), pp.51-58.
9. Johansen, J. and Sorensen, N.J., 'Prediction of laminar/turbulent transition in airfoil flows', AIAA-1998-0702.
10. Ekaterinaris, J.A., Srinivasan, G.R. and McCroskey, W.J., 'Present capabilities of prediction two-dimensional dynamic stall', Paper 2, AGARD CP 552, Berlin, 1994.
11. Ekaterinaris, J.A. and Platzer, M.F., '', Progress in Aerospace Science,
12. Hill, J.L., Shaw, S.T. and Qin, N., 'Investigation of transition modeling for aerofoil dynamic stall', in Proceedings of the 24th International Congress of the Aerospace Sciences, 2004.
13. Geissler, W. and Trenker, M., 'Numerical investigation of dynamic stall control by a nose-drooping device', Proc. American Helicopter Society , 2002.
14. Hill, J.L., Shaw, S.T. and Qin, N., 'Engineering prediction of laminar/turbulent transition for isolated helicopter rotors in hover', Royal Aeronautical Society Aerodynamics Research Conference, London, September 2004.
15. Wilcox, D.C., 'Turbulence modelling for CFD', DCW Industries, 1993.
16. Menter, F.R., 'Two-Equation Eddy-Viscosity Turbulence Models for Engineering Applications. AIAA Journal, Vol. 32 (8), 1994, pp. 1598-1605.
17. Osher, S. and Solomon, F., 'Upwind difference schemes for hyperbolic systems of conservation laws', Mathematics of computation, Vol. 38 (158), pp. 339-374.
18. Shaw, S.T. and Qin, N., 'Unsteady flow around helicopter rotor blade sections in forward flight', The Aeronautical Journal of the Royal Aeronautical Society, Vol. 103, pp. 35-44.
19. Qin, N., Ludlow, D.K. and Shaw, S.T., 'A matrix-free preconditioned Newton/GMRES method for unsteady Navier-Stokes solutions', Int. J. Numerical Methods in Fluids,Vol.33, pp.223-248.
20. Qin, N., Zhu, Y. and Shaw, S.T., 'Numerical study of active shock-control for transonic aerodynamics', International Journal of Numerical Methods for heat and fluid flow, Vol.14, No.4, 2004.
21. Qin, N., Ludlow, D.K., Shaw, S.T., Edwards, J.A., and Duquis, A. 'Calculation of pitch damping coefficients for a flared projectile', J. Spacecraft and Rockets, Vol. 34(4), 1997.
22. Thwaites, B., 'Approximate Calculation of the Laminar Boundary Layer', Aeronautical Quarterly, Vol 1, pp 245-280.
23. Krumbein, A., 'Transitional flow modeling and application to high-lift multi-element airfoil configurations', J. Aircraft, Vol. 40 (4).
24. Schmidt, G. S., Analysis of Low Reynolds Number Separation Bubbles Using Semi-empirical Methods. AIAA J., Vol. 27 (8).
25. Walker, G.J., 'Transitional flow on axial turbo-machinery blading', AIAA J., Vol. 27 (5).
26. Wilcox, D.C., 'Simulation of transition with a two-equation turbulence model', AIAA J., Vol. 32 (2).
27. Gregory, N. and O'Reilly, C.L., 'Low-speed aerodynamic characteristics of NACA 0012 aerofoil section, including the effects of upper-surface roughness simulating hoar frost', NPL Aero Report 1308, 1970.
28. Allain C. 'Contribution à l'étude expérimentale de la couche limite soumise à une instationnarité forcée. Application aux phénomènes de transition et de décollement en écoulement in stationnaire 2D/3D', PhD thesis, Université de la Méditerranée, 1999.
29. FavierD., Maresca C., Berton E., Allain C., 'Etude expérimentale et numérique du développement de la couche limite instationnaire sur modèles oscillants en écoulement 2D/3D.', DRET, Convention n°95-052, 1996.
30. Haase, W., Chaput, E., Elsholz, E., Leschziner, M.A. and Muller, U.R. (Editors), 'Validation of CFD codes and assessment of turbulence models', Notes on numerical fluid mechanics, Vol. 58, 1997.
31. Carr, L.W., 'Progress in Analysis and Prediction of Dynamic Stall', Journal of Aircraft, Vol. 25 (1), 1988, pp. 5-17.
32. Carr, L.W. and Chandrasekhara, M.S., 'Compressibility effects on Dynamic Stall', Progress in Aerospace Sciences, Vol. 32.
33. Beddoes, T.S., and Leishman, J.G., 'A semi-empirical model for dynamic stall', Journal of the American Helicopter Society, Vol. 34 (3), 1989.
34. Piziali, R.A., 'An experimental investigation of 2D and 3D oscillatory wing aerodynamics for a range of angle of attack including stall', NASA TM 4632, 1994.
35. McCroskey, W.J., 'The phenomena of dynamic stall', NASA TM 81264, 1981.
36. Shaw, S.T. and Hill, J.L., 'Apriori grid adaptation helicopter rotor wakes using structured-unstructured hybrid meshes', submitted for publication, 2004.

Caraddona F.X., and Tung, C., 'Experimental and analytical studies of a model helicopter rotor in hover', NASA TM-81232, 1981.